The G-protein Alpha Subunit Gsα Is A Tumor Suppressor In Sonic Hedgehog-driven Medulloblastoma

Published in final edited form as:
Nat Med. 2014 September ; 20(9): 1035–1042. doi:10.1038/nm.3666.

The G-protein Alpha Subunit Gsα Is A Tumor Suppressor In Sonic Hedgehog-driven Medulloblastoma

Xuelian He[1,2], **Liguo Zhang**[2], **Ying Chen**[3], **Marc Remke**[4], **David Shih**[4], **Fanghui Lu**[2], **Haibo Wang**[2], **Yaqi Deng**[2], **Yang Yu**[1], **Yong Xia**[5], **Xiaochong Wu**[4], **Vijay Ramaswamy**[4], **Tom Hu**[7], **Fan Wang**[1], **Wenhao Zhou**[6], **Dennis K. Burns**[7], **Se Hoon Kim**[8], **Marcel Kool**[9], **Stefan M. Pfister**[9], **Lee S. Weinstein**[10], **Scott L. Pomeroy**[11], **Richard J. Gilbertson**[12], **Joshua B. Rubin**[13], **Yiping Hou**[1], **Robert Wechsler-Reya**[14], **Michael D. Taylor**[4], and **Q. Richard Lu**[1,2,6,#]

[1]Department of Pediatrics and Obstetrics/Gynecology, School of Basic Science and Forensic Medicine, State Key Laboratory of Biotherapy/Collaborative Innovation Center for Biotherapy, West China Second Hospital, Sichuan University, Chengdu, China 61004

[2]Department of Pediatrics, Brain Tumor Center, Divisions of Experimental Hematology and Cancer Biology & Developmental Biology, Cincinnati Children's Hospital Medical Center, University of Cincinnati College of Medicine, Cincinnati, OH 25229, USA

[3]School of Life Sciences, Xiamen University, Fujian, China 361102

[4]The Hospital for Sick Children, University of Toronto, Toronto, ON M5G 1X8, Canada

[5]Department of Neurosurgery, West China Hospital, Sichuan University, Chengdu, Sichuan Province, China 61004

[6]Key Laboratory of Birth Defects, Children's Hospital of Fudan University, Shanghai, China, 201102

[7]Department of Pathology, University of Texas Southwestern Medical Center, Dallas, Texas 75390, USA

[8]Department of Pathology, Yonsei University College of Medicine, Seoul, Republic of Korea

[9]Division of Pediatric Neurooncology, German Cancer Research Center (DKFZ), 69121 Heidelberg, Germany

[10]Metabolic Diseases Branch, National Institute of Diabetes and Digestive and Kidney Diseases, NIH, Bethesda, Maryland, USA

[#] Correspondence: richard.Lu@cchmc.org Tel: 513-636-7684; Fax: 513-803-0783.

Author contributions

X. H., and Q. R. L. designed the experiments, analyzed the data and wrote the manuscript with input from all authors. X. H., L. Z., Y. C., M. R., D. S., F. L., H. W., Y. Y., Y. X., Y. D., V. R., X. W. and T. H. carried out the in vitro, in vivo, gene profiling or in silico studies. M. K. and S. M. P. provided whole-genome sequencing data. Y. H., F. W. and W. Z. provided resources and supervision. L.S.W. provided the *Gnas* floxed mice. D. K. B. and S. H. K. diagnosed and confirmed the *GNAS* mutated MB. S. L. P., R. J. G., J. B. R. and R. W-R provided conceptual advice and edited the manuscript. M. D. T. and Q. R. L. supervised the project.

Accession codes: The RNA-seq, mRNA affymetrix GeneChip microarray and aCGH microarray data are deposited in the NCBI Gene Expression Omnibus (GEO) under accession number GSE53248.

Competing Financial Interests

The authors declare no competing financial interests.

[11]Department of Neurology, Children's Hospital, Dana-Farber Cancer Institute, Harvard Medical School, Boston, Massachusetts 02115, USA

[12]Department of Developmental Neurobiology, St Jude Children's Research Hospital, Memphis, TN 38105, USA

[13]Departments of Pediatrics and Anatomy and Neurobiology, Washington University School of Medicine, St Louis, Missouri

[14]Tumor Development Program, Sanford-Burnham Medical Research Institute, La Jolla, CA 92037, USA.

Abstract

Medulloblastoma, the most common malignant childhood brain tumor, exhibits distinct molecular subtypes and cellular origins. Genetic alterations driving medulloblastoma initiation and progression remain poorly understood. Herein, we identify *GNAS*, encoding the G-protein Gsα, as a potent tumor suppressor gene that defines a subset of aggressive Sonic Hedgehog (Shh)-driven human medulloblastomas. Ablation of the single *Gnas* gene in anatomically-distinct progenitors is sufficient to induce Shh-associated medulloblastomas, which recapitulate their human counterparts. Gsα is highly enriched at the primary cilium of granule neuron precursors and suppresses Shh-signaling by regulating both the cAMP-dependent pathway and ciliary trafficking of Hedgehog pathway components. Elevation of a Gsα effector, cAMP, effectively inhibits tumor cell proliferation and progression in *Gnas* mutants. Thus, our gain- and loss-of-function studies identify a previously unrecognized tumor suppressor function for Gsα that acts as a molecular link across Shh-group medulloblastomas of disparate cellular and anatomical origins, illuminating G-protein modulation as a potential therapeutic avenue.

Keywords

medulloblastoma; G-protein; cAMP; GPCR; cell lineage; sonic hedgehog signaling; cilia; cellular origins

---

Medulloblastoma (MB) comprises clinically and molecularly distinct that arise either in the cerebellum or brainstem [1-3]. Although current treatments improve survival rates, patients suffer severe side effects and relapse of tumors carrying resistance mutations, underscoring an urgent need for alternative targeted therapies. Deregulation of G-protein coupled receptor (GPCR) pathways has been implicated in medulloblastoma [4-6], however, underlying signal transduction events that drive tumor initiation and progression remain obscure. *GNAS* encodes the heterotrimeric Gs protein alpha-subunit (Gsα) that functions as a molecular switch to transmit various GPCR signals to control cell growth, survival, and motility [7]. Recent genome-wide analyses of somatic mutations in cancers identified *GNAS* as one of the most frequently mutated genes [8]. Although most somatic tumor types acquire gain-of-function *GNAS* mutations [8], analysis of a copy number database (Tumorscape, Broad Institute) surprisingly reveals that MB displays a significant loss of the chromosomal region containing *GNAS* (**Supplementary Fig. 1**) compared to other cancers. Furthermore, a recent case report showed that a 14-month-old infant with a novel homozygous nonsense mutation

within the *GNAS* coding region developed MB [9]. Herein, we tested whether deregulation of Gsα-coding *GNAS* may contribute to MB formation.

Results

GNAS defines a subset of aggressive SHH-group tumors

Human MB can be classified into at least four principal subgroups, namely, WNT (Wingless) group, SHH (Sonic hedgehog) group, group 3 and group 4, based on distinct gene expression profiles [1]. To define the correlation of *GNAS* in MB subgroups, we examined *GNAS* expression from two independent, non-overlapping patient cohorts in the Boston and Heidelberg series [10-12]. We found that low *GNAS* expression was tightly correlated with significantly decreased overall survival within SHH-group tumors (SHH-MB), which comprise approximately 30% of all MBs [1] (**Fig. 1a,b**). Notably, the prognostic impact of *GNAS* was not observed in other group tumors and across MB subgroups (**Fig. 1c,d; Supplementary Figs. 2,3**). These observations suggest that low expression or loss of *GNAS* specifically defines a subset of aggressive SHH-group MBs.

Loss of *Gnas* in neural stem/progenitor cells induces MB formation with full penetrance

To determine whether *Gnas* inactivation could lead to brain tumorigenesis, we deleted *Gnas* in neural stem/progenitor cells by breeding floxed *Gnas* mice ($Gnas^{lox/lox}$) with an *hGFAP-Cre* line [13,14]. Strikingly, all resulting $hGFAP\text{-}Cre^{+/-}:Gnas^{lox/lox}$ conditional knockout mice (designated as *GFAP:Gnas*) developed MB-like tumors at adult stages (**Fig. 2a,b**). We observed expansion of granule neuron progenitors (GNPs) in the cerebellar external granular layer (EGL) beginning at neonatal stages, when the control cerebellum contained only a few rows of GNPs on its surface. Diffuse, continuous GNP expansion continued to increase at postnatal stages. *Gnas* mutant cerebella were exophytic and delineated by a thick and disorganized EGL (**Fig. 2a**). By six weeks, *GFAP:Gnas* mice developed a diffuse MB-like tumor exhibiting the densely-packed, “small round blue” GNP-like histology (**Fig. 2c**; inset), resembling the histological features of human MB [15]. In the mutants at P60, the neoplastic cells were highly proliferative as indicated by extensive expression of Ki67, a proliferative marker, which was barely detectable in controls (**Fig. 2d**). 100% of animals succumbed to the tumor around 3-4 months of age (**Fig. 2e**). Although the *hGFAP-Cre*-recombined cells appear in most brain regions [13], tumor formation was confined only to the cerebellum during the lifespan of *Gnas* mutants.

To ascertain gene expression alterations caused by *Gnas* loss, we examined mRNAs isolated from the cerebella of control and *GFAP:Gnas* mice at P60 by RNA-deep sequencing. In tumors of *Gnas* mutants, our data revealed an up-regulation of Shh signaling pathway components (**Fig. 2f**). Quantitative RT-PCR confirmed that expression of Shh target genes and pathway components was significantly up-regulated (**Fig. 2g**). Consistently, mRNA *in situ* hybridization revealed intense expression of Shh downstream genes including *Gli1, Gli2, Ptch1* and *cyclinD1* (*Ccnd1*) (**Fig. 2h**). Furthermore, we observed significant elevation of Shh direct target genes *Gli1* and *Ptch1* (**Fig. 2i**) in GNP-like tumor cells compared with normal GNPs, suggesting a cell-intrinsic effect of *Gnas* mutation on Shh signaling activation. By contrast, expression of Wnt-target genes was not substantially altered

(**Supplementary Fig. 4**), consistent with previous findings that *Gnas* loss does not affect Wnt signaling in other cellular systems [16]. We observed widespread expression of GNP markers Zic1 and Atoh1 (a.k.a. Math1), along with Shh-regulated targets including Olig2 [17], but very few astrocytic GFAP$^+$ astrocytes (**Fig. 2j**). Thus, *Gnas* loss results in an increase or alternatively a de-repression of physiological levels of Shh pathway activity and over-proliferation of GNP-like tumor cells.

Gsα activity suppresses hedgehog signaling

To test whether the GTPase activity of Gsα protein is required for inhibition of Shh signaling, we treated GNP cells isolated from wildtype neonates with NF449, a selective Gsα antagonist [18], which prevents GTP binding to Gsα and blocks Gsα GTPase activity. Treatment of NF449 resulted in a significant up-regulation of Shh target genes *Gli1*, *Gli2*, *Ptch1* and *Myc-N* and caused a decrease of cAMP levels (**Fig. 3a**), suggesting that inhibition of Gsα GTPase activity activates Shh signaling. To investigate the effect of Gsα gain-of-function activity on Shh signaling, we generated a constitutively activated form of Gsα, GsαQ227L (GsCA), which resulted in a GTPase-defective, active GTP-bound Gsα protein [19]. Overexpression of GsCA in GNPs suppressed the upregulation of Shh targets *Gli1*, *Ptch1*, *Myc-N* and *Ccnd1* induced by a Shh agonist SAG (**Fig. 3b**), indicating that Gsα activation inhibits hedgehog signaling.

Elevation of the Gsα effector cAMP inhibits MB growth

The classic signal transduction pathway of Gsα is through activation of adenylyl cyclase, which, in turn, produces intracellular cAMP [20]. cAMP has been shown to activate cAMP-dependent Protein Kinase A (PKA), a negative effector of Shh signaling [21-23]. Tumor cells isolated from *Gnas* mutants had a significant reduction in intracellular cAMP levels, while treatment with the adenylyl cyclase agonist forskolin (FSK) elevated cAMP levels (**Fig. 3c**). To test the hypothesis that cAMP elevation could inhibit Shh signaling activation, we treated *Gnas* mutant GNPs with Rolipram, which elevates cAMP levels by selectively inhibiting phosphodiesterase-4 activity to block cAMP degradation [24,25], FSK or a non-hydrolysable cAMP analog db-cAMP. Each of these cAMP-raising agents significantly reduced expression of *Gli1* and *Ptch1* (**Fig. 3d**). In addition, in wildtype GNPs, treatment with FSK and Rolipram enhanced the proteolytic processing of full-length Gli3 into a repressive form Gli3R (**Fig. 3d**), an inhibitor of Shh target expression [26,27]. In contrast, inhibition of cAMP-dependent PKA with two different small molecule inhibitors, H89 and KT570, significantly increased expression of *Gli1*, *Ptch1* and *Ccnd1* (**Fig. 3e**). Furthermore, mitigation of PKA activity by H89 (**Supplementary Fig. 5**) can restore Shh target expression suppressed by constitutively activated Gsα (**Fig. 3f**). Thus, our data are in keeping with previous observations that Gsα-mediated signaling can elevate cAMP levels to inhibit hedgehog target gene expression through cAMP-dependent PKA activity in other cellular systems [26,28,29].

To determine the effects of cAMP elevation on tumor growth in *vivo*, we evaluated the efficacy of Rolipram, which is well tolerated and readily crosses the blood brain barrier *in vivo* [24,30]. Control and *GFAP:Gnas* mutants at the young adult stage P35 were randomized to receive either daily i.p. vehicle or Rolipram for 30 days with a dosage exhibiting effective

anti-tumor activity *in vivo* [30], and assessed for tumor development. Rolipram administration during this period did not affect overall cerebellar structure and myelin formation (**Fig. 3g**; **Supplementary Fig. 6**). Vehicle-treated *Gnas* mutants displayed extensive tumor cell expansion and bulged cerebella (**Fig. 3g**). In contrast, in Rolipram-treated mutants, the tumor size and proliferation of $Zic1^+$ GNP-like tumor cells were substantially reduced (**Fig. 3g-i**). In addition, Rolipram treatment exhibited a significantly extended lifespan of *Gnas* mutants (**Fig. 3j**). Thus, elevation of the Gsα effector cAMP by Rolipram could lead to inhibition of tumor growth in *Gnas* mutants.

Gsα controls ciliary trafficking of hedgehog signaling components in GNPs

Ciliary trafficking of signaling components has an important role in regulating Shh pathway activity and MB formation [22,31,32]. Strikingly, we observed that Gsα was highly enriched at the primary cilium of GNPs (**Fig. 4a**) but hardly detectable in mouse embryonic fibroblasts (**Supplementary Fig. S7**), suggesting a unique ciliary function of Gsα for GNP development. In the presence of Shh, ciliary localization of Gsα is diminished (**Fig. 4a,b**). Treatment of Shh and its agonist SAG [33] did not alter the total amount of Gsα protein, but rather reduced the amount of the GTP-bound, active form of Gsα protein (Gsα-GTP; **Supplementary Fig. 8**).

In GNPs from *GFAP:Gnas* mutants, Gsα expression was essentially depleted, while total levels of Smoothened (Smo) were comparable to controls (**Supplementary Fig. 9**). At the tips of cilia, approximately 64.3 ± 6.2% cells exhibited strong immunoreactivity for Gli2, a Shh downstream effector (**Fig. 4c**, insets), whereas Gli2 was hardly detectable or weakly presented in control GNPs (**Fig. 4c,d**). Consistent with a principal function of PKA in restraining Gli2 activation [21,23], our observation suggests that *Gnas* loss reduces cAMP-dependent PKA activity and increases Gli2 accumulation at ciliary tips, leading to Shh signaling activation. We further detected ciliary translocation of Smo seven-transmembrane protein in the majority of *Gnas* mutants, but not in control GNPs, where Smo was diffusely localized in the cytoplasm near the base of cilia but absent from ciliary shafts (**Fig. 4e,g**). Conversely, a Smo-inhibiting protein, Ptch1, was mainly detected in the ciliary shaft of control GNPs (**Fig. 4f**) but absent from cilia in *Gnas* mutants (**Fig. 4f,g**). In contrast, ciliary trafficking of a Shh signaling regulator Gpr161[29] was not altered in *Gnas* mutants (**Supplementary Fig. 10**), suggesting a specificity of Gsα in regulating ciliary localization of GPCRs. Consistent with the existence of multiple Gsα-mediated GPCRs, $Gpr161^{-/-}$ embryos exhibited milder developmental defects than $Gnas^{-/-}$ animals [28]. Given that *PKA* null mutation could lead to Gli2 accumulation at the tips of cilia, but not the ciliary trafficking of Smo in neural progenitors [21], our observations of both strong Gli2 signal at the ciliary tip and Smo ciliary translocation in *Gnas* mutants suggest that Gsα might have an additional role in regulating Smo trafficking in primary cilia independent of cAMP-dependent PKA activity.

cAMP elevation and Smo inhibition augment suppression of tumor cell proliferation

Our data indicate that Gsα suppresses Shh signaling not only by stimulating intracellular cAMP levels to activate PKA, but also perhaps independently by inhibiting Smo activation. Treatment of *Gnas* mutant GNPs with GDC-0449, which blocks SMO activation induced by

SAG (**Supplementary Fig. 11**)[34], led to a reduction in *Gli1* and *Ptch1* expression (**Fig. 4h**). Combined treatment of GDC-0449 and Rolipram however resulted in further inhibition of Shh target expression (**Fig. 4h**). Since *Gnas* mutant GNPs are highly proliferative (**Fig. 4i**), we then determined whether cell proliferation is responsive to cAMP elevation and Smo inhibition. The proliferation rate was reduced in *Gnas*-mutant GNPs treated with Rolipram or GDC-0449 to a certain extent, where Rolipram exhibited a relatively stronger effect than GDC-0449 (**Fig. 4i,j**). However, combinatorial treatment of both drugs was found to cause a greater inhibition of cell proliferation in *Gnas* mutants (**Fig. 4i,j**).

Loss of *Gnas* in *Atoh1*$^+$ or *Olig1*$^+$ progenitors leads to anatomically distinct MBs

SHH-driven MBs may arise from multiple cellular origins in human patients [3]. hGFAP-Cre mediated *Gnas* deletion might affect multiple progenitor populations in the posterior fossa. To examine whether *Gnas* loss in committed GNPs could result in MB formation, we crossed *Gnas*floxed mice with an Atoh1-Cre line, which directs Cre expression in GNPs of the cerebellum and dorsal brainstem cochlear nuclei [3,35]. The resulting *Atoh1-Cre*$^{+/-}$*:Gnas*$^{lox/lox}$ (*Atoh1:Gnas*) mutant mice developed MB-like tumors with an expansion of tumor cells in the EGL layer (**Fig. 5a**). Tumor cells expressed neuronal markers Tuj1 and Zic1 extensively with few Olig2 and GFAP-expressing glial cells (**Fig. 5b**), and exhibited a significant up-regulation of Shh signaling target genes *Ptch1*, *Gli1* and *Hhip* (**Fig. 5c**). This suggests that ablation of *Gnas* selectively in committed cerebellar GNPs is sufficient to cause Shh-associated MB formation.

To test whether other Shh-responsive progenitor cells were susceptible to oncogenic transformation due to *Gnas* loss, we ablated *Gnas* in the progenitors expressing a Shh-regulated gene *Olig1*[36,37]. During embryogenesis, *Olig1* is mainly expressed in the specified progenitors of the brainstem around rhombomeres r2-r4, which can give rise to oligodendrocyte precursors (OPC) and granule neuron lineage cells [37,38] (**Fig. 5d**). The *Olig1*$^+$ progenitors were mainly detected in the rostral brainstem but separated from caudal brainstem progenitors in rhombomeres r6-r8, a source of Wnt-associated MBs [39] (**Fig. 5d**). They were essentially undetectable in the upper rhombic lip, EGL and cochlear nucleus (**Fig. 5d**; **Supplementary Fig. 12**), the other sources for Shh-associated MBs [3,35]. Lineage tracing analysis indicated that the progeny of *Olig1*$^+$ progenitors were present in a population of Zic1$^+$ GNPs in the dorsal brainstem (**Fig. 5e**). Notably, *Olig1-Cre*$^{+/-}$*:Gnas*$^{lox/lox}$ mutant mice (designated as *Olig1:Gnas*) generated by breeding *Gnas*-floxed and *Olig1-Cre* mice developed anatomically-distinct tumors that were largely restricted between the caudal posterolateral lobe and the dorsal brainstem around the fourth ventricle (**Fig. 5f**), and contiguous within the rostral brainstem (**Fig. 5g**). *Olig1:Gnas* mice developed relatively intact cerebellar structure and morphology, displaying tumor formation around 3 months of age. Approximately 37.4 ± 4.1% of cells in the tumor tissues expressed Ki67 (**Fig. 5h**), suggesting that the neoplastic cells are highly proliferative. In tumors of *Olig1:Gnas* mice, we detected extensive expression of the neuronal markers NeuN, Zic1 and Pax6 (**Fig. 5i**), a hallmark feature of a primitive neuroectodermal tumor-like MB [40]. In contrast, only a few scattered cells in the tumor were positive for an astrocytic marker GFAP (**Fig. 5j**).

Anatomically-distinct tumors from different *Gnas* mutants resemble SHH-associated MB

Although the localization of MBs is distinct between *Olig1:Gnas* and *GFAP:Gnas* mutants (**Fig. 1**), transcriptome profiling by RNA-seq (**Fig. 6a**) and qRT-PCR (**Fig. 6b**) analysis revealed a significant up-regulation of Shh pathway components in tumors of either origin. Regression analysis reveals a direct correlation of gene transcription profiles between *GFAP:Gnas* and *Olig1:Gnas* tumors (**Fig. 6c**). Cross-species comparison of gene expression profiles of *Gnas* tumors with data from human MB subgroups using two different class prediction algorithms AGDEX[41] (**Fig. 6d,e**) and PAM[42] (**Fig. 6f**) revealed that the tumors derived from both *GFAP:Gnas* and *Olig1:Gnas* mice showed a gene expression signature most closely resembling the SHH-group human MB (**Fig. 6df**). Therefore, our data highlight *Olig1*$^+$ progenitors in the posterior fossa as an important source of a subset of Shh-associated MBs with heterogeneous cellular origins[3].

To further examine the tumorigenic capacity of neoplastic cells in these *Gnas* mutants, we transplanted cells isolated from tumor tissues from *GFAP:Gnas* or *Olig1:Gnas* mutants by stereotactically injecting them into the forebrain in immuno-compromised nude mice. Tumor cells were able to propagate into the brain in the transplanted animals and became obvious one month after transplantation (**Supplementary Fig. 13**). Tumors formed in mouse allografts persisted with GNP-like tumor cells exhibiting MB histology (**Supplementary Fig. 13**). Congruent with gene profiling and histological data, this suggests that the tumors in *GFAP:Gnas* or *Olig1:Gnas* mutants comprise transformed neoplastic cells, resembling SHH-driven MBs. Moreover, to identify the subgroup affiliation of MB in the patient with a homozygous *GNAS*-inactivating mutation [9], we carried out targeted gene-expression profiling analysis and observed a significant upregulation of signature genes in the SHH-group but not in WNT, group 3 or 4 MB (**Fig. 6g**). Thus, our results predict that the tumor carrying the *GNAS* nonsense mutation is a SHH-subgroup MB with high confidence (**Fig. 6g**). Furthermore, a recent genome sequencing study identified eight cases out of 133 SHH-MBs carrying *GNAS* mutations including one case with a frame-shift mutation [5] (**Supplementary Table 1**). Together with tumor formation in *Gnas* mutants, these studies suggest that *GNAS* inactivating mutations could lead to SHH-MB formation in patients.

Discussion

We demonstrate here that the *Gnas*-encoded GPCR signal transducer Gsα is a potent tumor suppressor in Shh-driven MBs. *Gnas* expression determines progenitor cell competency in initiation of MBs among distinct cells of origin. Low levels of *GNAS* define a subset of aggressive SHH-MB, highlighting *GNAS* as a prognostic biomarker for treatment stratification of SHH-associated tumors. The case report that the patient with a homozygous *GNAS* nonsense mutation [9] developed SHH-MB provides additional clinical relevance of *GNAS* deregulation in tumor formation. Our gain- and loss-of-function studies suggest that Gsα inhibits MB formation at least in part by suppressing Shh signaling through activating the cAMP-dependent pathway to regulate Gli3 processing and Gli2 activation, as well as modulating ciliary trafficking of hedgehog signaling components in GNPs. Thus, a dual-mode regulation of the intracellular cAMP signaling cascade and Smo activation at the primary cilium by Gsα reinforces the inhibition of Shh signaling and blocks MB initiation.

Our data further suggest that Gsα might serve as a point of convergence between Smo and various Gsα-coupled GPCR signaling pathways [4,6,29,43] to modulate Shh signal strength and control MB formation. We did not detect significant alterations of gene loci encoding hedgehog-pathway components such as *PTCH1*, *SMO* or *SUFU* in *GNAS*-low SHH-MBs [44] and in *Gnas* tumors (**Supplementary Fig. 14, Table 1**), suggesting that *GNAS* deregulation or inactivation may represent a unique subset of SHH-MBs. Nonetheless, our copy number variation study revealed a number of other genetic alterations occurred in both *GFAP:Gnas* and *Olig1:Gnas* mutants. The altered genetic loci harboring homozygous deletions include *Tulp4*, a candidate tumor suppressor gene in MB [39] and *Hjurp*, a critical factor for chromosome segregation and stability [45,46] (**Supplementary Fig. 14**). These genetic alterations might potentially contribute to transforming mechanisms in *Gnas* mutants.

We identify *Olig1*$^{+}$ progenitors as a cellular source for Shh-associated tumors localized to the dorsal brainstem, demonstrating the cellular and anatomic heterogeneity within SHH-MB [2,3,5,47]. Recent studies indicate that Olig1 may regulate the fate switch between OPC and cerebellar interneurons [48], raising the possibility that interneuron precursors might contribute to MB formation. However, this seems unlikely because Shh-driven MBs are derived from lineage-restricted GNPs even with SmoM2 activation or *Ptch1* mutation in multipotent cerebellar progenitors [13,35]. Intriguingly, the ventral brainstem of *GFAP:Gnas* mice exhibits an expanded pontine grey nucleus derived from lower rhombic lip progenitors, which could also act as a source of Wnt-subgroup tumor [39]. Thus, Gsα may suppress MB formation in different types of progenitor cells. Together, our studies uncover *Gnas* as a potential molecular link among anatomically distinct MBs, pointing to a previously unrecognized tumor suppressor function of *Gnas* in the initiation of diverse MBs in light of other tumor types often caused by activating *GNAS* mutations [8,49].

Although Smo inhibitors show efficacy regarding the inhibition of MB growth in animal models such as *Ptch1* mutants [50] and adult Shh-driven MB patients [51], drug responses were only transient due to the emergence of drug resistance. Our data suggest that the cAMP stimulants such as Rolipram, which possesses anti-tumor activity and is clinically approved already as an antidepressant in humans in Japan and Europe [52], might be a potent alternative agent against aggressive SHH-MBs caused by *GNAS* inactivation. Although other cAMP raising agents have been previously proposed for the treatment of human tumors exhibiting overactive Shh pathways [52], our current spontaneous MB model with *Gnas* inactivation provides important and novel validation of the efficacy of Rolipram *in vivo*. This suggests that Rolipram and perhaps other cAMP-raising agents including bioflavonoids, which overcome multi-drug resistance in cancer therapy [53,54], might be repurposed for treating MB. The profound and specific impact of Gsα on MB tumorigenesis illuminates a new alternative treatment avenue, such that co-targeting of Gsα or its signaling effectors together with Smo inhibition might circumvent the drug resistance seen with Smo antagonists alone [51,55] and could be beneficial in treatment of aggressive SHH-MB with *GNAS* deregulation.

Online Methods

Animals

We bred *Gnas*$^{lox/lox}$ mice [56] with *hGFAP-Cre* (Jackson laboratory), *Atoh1-Cre* (gift from Dr. Bernd Fritzsch, University of Iowa) and *Olig1-Cre* [36] mice to generate *hGFAPCre*$^{+/-}$*:Gnas*$^{lox/+}$, *Atoh1Cre*$^{+/-}$*;Gnas*$^{lox/+}$ mice and *Olig1Cre*$^{+/-}$*;Gnas*$^{lox/+}$ mice, respectively, which were then bred with *Gnas*$^{lox/lox}$ mice to produce control mice (*hGFAPCre*$^{+/-}$*:Gnas*$^{lox/+}$, *Atoh1Cre*$^{+/-}$*;Gnas*$^{lox/+}$ and *Olig1Cre*$^{+/-}$*:Gnas*$^{lox/+}$), and *Gnas* mutant offspring *hGFAPCre*$^{+/-}$*:Gnas*$^{lox/lox}$ (*GFAP:Gnas*), *Atoh1-Cre*$^{+/-}$*:Gnas*$^{lox/lox}$ (*Atoh1:Gnas*) and *Olig1Cre*$^{+/-}$*;Gnas*$^{lox/lox}$(*Olig1:Gnas*) mice, respectively. The above control mice developed and behaved the same as wildtype. Rosa-tdTomato reporter mice (Jackson laboratory) and Atoh1-GFP reporter line (gift from Dr. Jane Johnson) were also bred with *Gnas* mutants to monitor gene deletion and Atoh1-expressing GNP cells, respectively. We used both male and female mice for the study. The mouse strains used in this study were generated and maintained on a mixed C57Bl/6;129Sv;CD-1 background. BALB/c nude mice (Charles River Laboratories) were used for allograft transplantation study. All animal use and studies were approved by the Institutional Animal Care and Use Committee of the University of Texas Southwestern Medical Center, Cincinnati Children's Hospital Medical Center, USA and animal use committee at Sichuan University in Chengdu, China. All human patient samples were obtained with consent as outlined by individual institutional review boards.

Tissue processing, antibodies, immunostaining and microscopy

Mouse brains at defined ages were dissected and fixed overnight in 4% (w/v) paraformaldehyde (PFA) and processed for cryosectioning or paraffin embedding and sectioning. The procedure for immunostaining was described previously [37]. Briefly, for tissue immunostaining, cryosections or pre-deparaffinized tissue sections were incubated overnight in primary antibodies diluted in block solution (PBS with 5% v/v normal goat serum (Sigma-Aldrich) and 0.3% v/v Triton X-100). After washing with PBS for five times, sections were then incubated overnight in appropriate either biotinylated secondary antibodies, followed by using the ABC avidin/biotin method to visualize staining signals under light microscopy with the peroxidase/diaminobenzidine (DAB) method, or incubated with corresponding fluorophore-conjugated secondary antibodies (Jackson ImmunoResearch) under fluorescent microscopy. For cell immunostaining, cultured cells were fixed with 4% PFA for 10 min and washed five times with PBS, then placed in blocking solution for 30 min. We incubated primary antibodies in blocking solution with proper dilutions and stain cells for 1 h at room temperature. For BrdU staining, cells or tissue sections were denatured with 0.1N HCl for 1 h in 37°C water bath. After denaturation, sections were neutralized with 0.1 M Borax, pH 8.5 (Sigma) for 10 min. Sections were washed with 0.3% Triton X-100/1 × PBS (wash buffer) for 3 times and blocked with 5% normal donkey serum (Sigma-Aldrich) contained wash buffer for 1 h at room temperature. Mouse-anti BrdU (BD Bioscience, 1:500) antibody was used to label BrdU overnight at 4°C. DAPI was included in the final washes before the samples were mounted in Fluoromount G (SouthernBiotech) for microscopy. Primary antibodies used in this study were as follows: Zic1 (Rockland, 200-401-159), Olig2 (gift of C. Stiles, Harvard Medical

School), GFAP (Sigma, G3893), Gsα (Santa Cruz, Sc-823), Smoothened (Smo) (LS-C47301, LSBio), acetylated α-tubulin (mAb 6-11B-1, Sigma), Patched1 (gift of Rajat Rohatgi, Stanford University), Gpr161 (gift of Suzie Scales, Genentech, Inc), Ki67 (Thermo Sci, Clone: SP6), Pax6 (Developmental Studies Hybridoma Bank-University of Iowa), Tuj1 (Covance, MMS-435P), BrdU (BD Bioscience 347580), NeuN (Millipore, MAB377), Arl13b (Santa Cruz, sc-102318), Gli2 and Gli3 (gift of Suzie Scales, Genentech, Inc.).

For microscopy and image acquisition, images of stained samples used in figures were collected on an inverted laser scanning confocal microscope (Carl Zeiss LSM 510) microscope equipped with high-efficiency fluorochrome specific filter sets for DAPI, Cy2, Cy3 and Cy5. For quantification of the number of Ki67, BrdU or Zic1-expressing cells, areas to be counted were traced with a 40× objective lens and sample frames (40 μm × 40 μm) were selected at least 10 random but non-overlap regions per section by the image analysis software. At least five sections at different hindbrain levels per animal were selected for quantification. Imaging of cilia was taken with a Zeiss immersion oil objective lens (63 ×) with 2× optical zoom magnifications. Experiments were performed at least three times for each genotype. At least 300 cells with visible cilia from each independent experiment per genotype were analyzed. Images were quantified in a double-blinded manner.

RNA *in situ* hybridization of brain sections was performed using digoxigenin-labeled riboprobes as described previously [17]. The probes used were: murine *Ptch1, Gli1, Gli2* and *Cyclin D1*. Detailed protocols are available upon request.

Cerebellar GNP culture and proliferation assays

Cerebella from P6 or P7 mice were digested with Trypsin/DNase (1 mg ml^{-1}; Worthington), triturated to obtain a single-cell suspension, and then centrifuged through a 35%–65% Percoll gradient (Sigma) according to Yang et al., 2008 [13]. Cells from the 35%–65% interface were suspended in the GNP culture medium [Neurobasal (Gibco) with 2 mM L-glutamine, 0.45% D-glucose, B27 supplement, 16 μg ml^{-1} N-Acetyl-LCysteine and penicillin/streptomycin]. We pre-plated GNPs onto poly-D-lysine (100 μg ml^{-1}) coated plates for 1 hr at 37°C twice, and then transferred them to Poly-D/L-ornithine coated plates for culture. We treated GNP cells from control and Gsα mutants with following agents: SAG (Enzo, Lx-270-426) 200 nM; forskolin (Sigma, F3917) 10 μM; a selective Gαs antagonist NF449 (http://www.tocris.com/dispprod.php?ItemId=1801#.UwpK4v3j7Ko) (Tocris, Cat. # 1391) 200 μM; GDC-0449 (Selleckchem, S1082) 1 μM and Rolipram 50 μM (R&D, Cat.# 0905) or transfected the cells with pcDNA3 or pGsCA for 48 hr. For *in vitro* proliferation assays, we labeled GNP cells with BrdU (50 μg ml^{-1}) for 48 hr followed by immunostaining.

Real-time RT-PCR Analysis

RNAs were isolated with the RNeasy Plus Mini kit (Qiagen) from GNP cells or snap-frozen tumors. Reverse transcription was performed with a High Capacity cDNA Reverse Transcription Kit (Applied Biosystems). We analyzed each gene with at least two different primer sets. qRT-PCR was carried out using the ABI Prism 7700 Sequence Detector System

(Perkin-Elmer Applied Biosystems) using *Gapdh* (TaqMan kit, Applied Biosystems) as an internal control. Each analysis was performed in triplicate, and the results were normalized to *Gapdh* for each sample. The primer sequences for qRT-PCR are available upon request.

Western blotting

GNP cells were rinsed in PBS and lysed in modified RIPA buffer (50 mM Na-Tris, pH 7.4, 150 mM NaCl, 1% (v/v) NP-40, 0.25% sodium deoxycholate, 1 mM dithiothreitol, 10 mM NaF, 1 mM active sodium vanadate, 1 mM PMSF and 1 × a cocktail of cOmplete protease inhibitors (Roche Applied Science) and centrifuged at 13,000 rpm for 15 min at 4 C. After the determination of protein concentration (Bio-Rad), the lysates were separated by 4–12% SDS-PAGE. We performed western blotting using standard protocols. The antibodies used were as follows: rabbit antibodies to Gli3 for detecting Gli3FL and Gli3R forms (gift of Suzie Scales), Gsα (Santa Cruz, Sc-823), anti-phospho-PKA substrates (P-PKAs, Cell Signaling, 9624s) and GAPDH (Santa Cruz, FL-335). Bands were visualized with secondary antibodies conjugated to horseradish peroxidase (Bio-Rad) and ECL western blotting detection reagents (Pierce) per the manufacturer's instructions. We used ImageJ densitometry software for western blot quantification.

Assay for activated Gsα (Gsα-GTP)

We performed activated Gsα-GTP pull-down assays following the manufacturer's protocol (NewEast Bioscience, 80801). Briefly, GNPs were incubated with Shh (3 μg ml^{-1}, R & D), XAV-939 (1 μM) and SAG (200 nM) for 1 h. Cell lysates were incubated with the antibody against the active form Gsα-GTP followed by protein A/G agarose beads for 1 h. Activated Gsα and Gsα proteins were detected by western blot with Gsα antibody.

Enzyme-linked immunoassay (ELISA) for cAMP

We plated GNP cells on 96-well tissue culture plates and cultured them for 1 day. The cAMP level in the GNPs was assayed following the manufacturer's protocol (Cell Signaling, 4339). In brief, GNPs were treated with SAG (200 nM), NF449 (100 μM) or forskolin (10 μM) for 24 hr. The amount of cAMP in lysates from 8,000 GNP cells was measured by ELISA.

RNA-seq data analysis

We isolated RNAs from the cerebella of adult wildtype mice and tumor tissue from individual *GFAP:Gnas* or *Olig1:Gnas* mutants and subject to RNA deep sequencing. RNA-seq libraries were prepared using Illumina RNA-seq Preparation Kit (Illumina) and sequenced in HiSeq 2000 sequencer. RNA-seq reads were mapped using TopHat with default settings. TopHat output data was then analyzed by Cufflinks to (1) calculate FPKM values for known transcripts in mouse genome reference and (2) test for changes of gene expression of control and tumor tissues.

Copy number variation analysis

We isolated genomic DNAs from the cerebellum of adult wildtype mice and tumor tissue from individual *GFAP:Gnas* or *Olig1:Gnas* mutants (n = 3 for each genotype) using a DNA

preparation kit (Zymo Inc.) and were hybridized on aCGH arrays (Nimblegen, Mouse CGH 3x720K Whole-Genome Tiling Array) according to the manufacturer's protocol. Data from the aCGH arrays were analyzed using the Nexus aCGH software with recommended normalization settings. Each sample was compared to a distributed baseline to identify amplified and deleted regions using a segmentation algorithm within Nexus Suite using a cutoff with gain (≥ 0.23) and loss (≤ –0.5) and significance threshold = 1.0E–5. Segments showing copy number variation were only reported if they occurred in list those regions of gain or loss with an individual False Discovery Rate (FDR) no greater than 5%.

Classification of medulloblastoma patient subgroups

Classification of a group of 103 paraffin-embedded MB samples was established using unsupervised hierarchical clustering (HCL) as the training series described previously [57,58]. Unsupervised HCL of MB expression data identified the following four unique sample clusters: WNT group, SHH group, group C, and group D. Briefly, gene expression data from MB patient samples were generated by using Affymetrix_HTHGU133Achips (Affymetrix, Santa Clara, CA). Molecular subgroups were classified using TM4 Microarray Software Suite (MeV v4.4; Dana-Farber Cancer Institute, Boston, MA). Subgroup-specific signature genes were identified by a multivariate permutation test. We performed principal component analysis (PCA) of gene expression data using Partek Genomics Suite (Partek, St Louis, MO).

Subgroup determination of the tumor with a homozygous *GNAS* nonsense mutation from a 14-month-old post-mortem infant: Total RNA was extracted from FFPE tumor tissue using the Qiagen RNeasy FFPE Kit (Qiagen, Hilden, Germany) and 200 ng of total RNA were analysed on a nanoString nCounter using a custom 25 gene probeset as previously described [58]. Counts were normalized to the three housekeeping genes (*GAPDH*, *ACTB* and *LDHA*) and subgroup prediction was done using PAM (Prediction analysis of microarrays) as previously described using the R-statistical environment (v2.15.1)[58].

Molecular classification of mouse tumors

Mouse tumors and normal cerebella (n = 8 each group) were profiled on the Affymetrix GeneChip Mouse Gene 1.1 ST v1 platform. Transcript level Robust Multi-array Average (RMA) normalization was performed using the oligo package (v 1.14) [59] in the R environment (v 2.15). Mouse transcripts were mapped to Human transcripts using gene orthology predicted by EnsemblCompara GeneTrees[60] available on Ensembl BioMart (GRCm38 dataset). Subsequently, the expression profiles were analyzed to assign molecular MB subgroup to the mouse tumors, using the AGDEX R package (v 1.0.1) [41] and human MB expression data from Northcott et al [57]. In this cross-species comparison of global differential expression, mouse normal cerebellum and human normal cerebellum were used as references. The degrees of agreement in differential expression of the mouse tumors between each of the four human MB subgroups were assessed separately and tested for statistical significance using permutation tests.

The molecular classification of the mouse tumors were also performed using a class prediction algorithm, Prediction Analysis for Microarrays (PAM)[42], as implemented in the

pamr package (v 1.51). The mouse and human samples first were normalized to their respective cerebellar references. Subgroup-specific markers were identified based on Kruskal-Wallis tests with multiple hypothesis correction by the Benjamin-Hochberg method, using a false discovery rate threshold of 0.01 and a signal-to-noise ratio threshold of 1.5. The resulting 545 subgroup-specific signature markers were used as features for class prediction of the mouse tumors using a PAM classifier trained on the human MB samples. Predicted subgroups with confidence probabilities higher than established thresholds [58] were considered bona fide subgroup assignments. Plots were generated by Principal Component Analyses (PCA) on the expression profiles of human medulloblastomas (training data). The resulting eigen vectors were used to project the expression profiles of the classified samples onto the vector space spanned by the first two eigen vectors of the training data. The background confidence score gradient was generated using 200 replicates of the training data with added Gaussian noise and subsequently smoothed by Nadaraya-Watson normalization (fields v6.7.6 R package).

Rolipram treatment in mice and volumetric measurement of tumors

Control and *GFAP:Gnas* mutant mice at P30-P35 were randomized to receive either Rolipram (5 mg kg^{-1}) or vehicle control [5% (v/v) DMSO] administered twice daily via intraperitoneal injection as previously described [30]. Brain tissues were harvested and processed into 8-μm sections in the sagittal plane and stained with hematoxylin and eosin (H/E) or subject to immunostaining. Abnormal tissue area with densely packed cells and round-to-oval hyperchromatic nuclei was assumed to be tumor tissue in the tissue section. For volumetric measurement, sections of cerebella were scanned by using a ScanScope XT from Aperio (Vista, CA) to acquire serial section images, then stacked and aligned with the StackReg function of ImageJ to generate three-dimension models and analyzed with Imaris Software (Bitplane) to calculate the volume of tumor tissues.

Intracranial transplantation

Tumor cells isolated from Gsα mutants were plated in GNP culture medium, and harvested with 0.25% trypsin and 0.02% EDTA for 2 minutes, washed twice with Hank's balanced salt solution (HBSS), and resuspended in Ca^{2+} and Mg^{2+}-free HBSS. Cell viability was determined by trypan blue exclusion. Only single-cell suspensions with more than 90% viability were used for *in vivo* allograft studies. Cells (5×10^5) were stereotactically injected into the lateral ventricle of nude mice (6-week-old BALB/c nu/nu; coordinates: anterior–posterior, +1.8; medial–lateral, +2.2; dorsal–ventral, -2.0 mm from Bregma).

Statistical analysis

All analyses were done using Microsoft Excel or Prism GraphPad 6.00 for Mac OS (San Diego California, www.graphpad.com). Quantifications were performed from at least three independent experimental groups. Data are presented as mean ± S.E.M. in the graphs. *p*-values are from Student's two-tailed *t* test to compare two sets of data. To compare more than two sets, one-way analysis of variance analysis (ANOVA) with a Newman–Keuls multiple comparison test for post-hoc analysis. Survival analyses used animal death times and censoring times when animals were sacrificed or as otherwise stated. Survival curves

were plotted with the Kaplan– Meier method and compared by using a two-sided log-rank test. In human tumor data analysis, Fisher's exact test was used for data in Tumorscape database unless otherwise specified. $p < 0.05$ is considered to be statistically significant.

Supplementary Material

Refer to Web version on PubMed Central for supplementary material.

Acknowledgements

The authors would like to thank A. Gilman, L. Lum, E. Hurlock, K. Campbell, J. Chan, H. Li, A. Hassan, D. He, E. Lu and W. Ding for comments and technical support. We thank B. Fritzsch (U. Iowa) for Atoh1-Cre line, R. Rohatgi (Stanford U.) for Ptch1 antibody and S. Scales (Genentech Inc.) for Gli2, Gli3 and GPR161 antibodies. This study was funded in part by grants from the US National Institutes of Health (R01 NS078092 and R01 NS075243) to QRL and from Canadian Institutes of Health Research (CIHR) to MDT, and postdoctoral fellowship by the Mildred-Scheel foundation/German Cancer Aid (MR).

References

1. Taylor MD, et al. Molecular subgroups of medulloblastoma: the current consensus. Acta neuropathologica. 2012; 123:465–472. doi:10.1007/s00401-011-0922-z. [PubMed: 22134537]
2. Northcott PA, et al. Pediatric and adult sonic hedgehog medulloblastomas are clinically and molecularly distinct. Acta neuropathologica. 2011; 122:231–240. doi:10.1007/s00401-011-0846-7. [PubMed: 21681522]
3. Grammel D, et al. Sonic hedgehog-associated medulloblastoma arising from the cochlear nuclei of the brainstem. Acta neuropathologica. 2012; 123:601–614. doi:10.1007/s00401-012-0961-0. [PubMed: 22349907]
4. Sasai K, et al. Medulloblastomas derived from Cxcr6 mutant mice respond to treatment with a smoothened inhibitor. Cancer research. 2007; 67:3871–3877. [PubMed: 17413002]
5. Kool M, et al. Genome Sequencing of SHH Medulloblastoma Predicts Genotype-Related Response to Smoothened Inhibition. Cancer cell. 2014; 25:393–405. doi:10.1016/j.ccr.2014.02.004. [PubMed: 24651015]
6. Niewiadomski P, Zhujiang A, Youssef M, Waschek JA. Interaction of PACAP with Sonic hedgehog reveals complex regulation of the hedgehog pathway by PKA. Cellular signalling. 2013; 25:2222–2230. doi:10.1016/j.cellsig.2013.07.012. [PubMed: 23872071]
7. Neves SR, Ram PT, Iyengar R. G protein pathways. Science. 2002; 296:1636–1639. doi:10.1126/science.1071550. [PubMed: 12040175]
8. Kan Z, et al. Diverse somatic mutation patterns and pathway alterations in human cancers. Nature. 2010; 466:869–873. doi:10.1038/nature09208. [PubMed: 20668451]
9. Huh JY, et al. Novel nonsense GNAS mutation in a 14-month-old boy with plate-like osteoma cutis and medulloblastoma. The Journal of dermatology. 2014 doi:10.1111/1346-8138.12284.
10. Cho YJ, et al. Integrative genomic analysis of medulloblastoma identifies a molecular subgroup that drives poor clinical outcome. J Clin Oncol. 2011; 29:1424–1430. doi:10.1200/JCO.2010.28.5148. [PubMed: 21098324]
11. Remke M, et al. Adult medulloblastoma comprises three major molecular variants. J Clin Oncol. 2011; 29:2717–2723. doi:10.1200/JCO.2011.34.9373. [PubMed: 21632505]
12. Remke M, et al. FSTL5 is a marker of poor prognosis in non-WNT/non-SHH medulloblastoma. J Clin Oncol. 2011; 29:3852–3861. doi:10.1200/JCO.2011.36.2798. [PubMed: 21911727]
13. Yang ZJ, et al. Medulloblastoma can be initiated by deletion of Patched in lineage-restricted progenitors or stem cells. Cancer cell. 2008; 14:135–145. [PubMed: 18691548]
14. Zhuo L, et al. hGFAP-cre transgenic mice for manipulation of glial and neuronal function in vivo. Genesis. 2001; 31:85–94. [PubMed: 11668683]

15. Northcott PA, Korshunov A, Pfister SM, Taylor MD. The clinical implications of medulloblastoma subgroups. Nat Rev Neurol. 2012; 8:340–351. doi:10.1038/nrneurol.2012.78. [PubMed: 22565209]
16. Regard JB, et al. Wnt/beta-catenin signaling is differentially regulated by Galpha proteins and contributes to fibrous dysplasia. Proceedings of the National Academy of Sciences of the United States of America. 2011; 108:20101–20106. doi:10.1073/pnas.1114656108. [PubMed: 22106277]
17. Lu QR, et al. Common developmental requirement for Olig function indicates a motor neuron/oligodendrocyte connection. Cell. 2002; 109:75–86. [PubMed: 11955448]
18. Hohenegger M, et al. Gsalpha-selective G protein antagonists. Proceedings of the National Academy of Sciences of the United States of America. 1998; 95:346–351. [PubMed: 9419378]
19. Graziano MP, Gilman AG. Synthesis in Escherichia coli of GTPase-deficient mutants of Gs alpha. The Journal of biological chemistry. 1989; 264:15475–15482. [PubMed: 2549065]
20. Dorsam RT, Gutkind JS. G-protein-coupled receptors and cancer. Nature reviews. Cancer. 2007; 7:79–94.
21. Tuson M, He M, Anderson KV. Protein kinase A acts at the basal body of the primary cilium to prevent Gli2 activation and ventralization of the mouse neural tube. Development. 2011; 138:4921–4930. doi:10.1242/dev.070805. [PubMed: 22007132]
22. Nozawa YI, Lin C, Chuang PT. Hedgehog signaling from the primary cilium to the nucleus: an emerging picture of ciliary localization, trafficking and transduction. Current opinion in genetics & development. 2013 doi:10.1016/j.gde.2013.04.008.
23. Pan Y, Wang C, Wang B. Phosphorylation of Gli2 by protein kinase A is required for Gli2 processing and degradation and the Sonic Hedgehog-regulated mouse development. Developmental biology. 2009; 326:177–189. doi:10.1016/j.ydbio.2008.11.009. [PubMed: 19056373]
24. Nikulina E, Tidwell JL, Dai HN, Bregman BS, Filbin MT. The phosphodiesterase inhibitor rolipram delivered after a spinal cord lesion promotes axonal regeneration and functional recovery. Proceedings of the National Academy of Sciences of the United States of America. 2004; 101:8786–8790. [PubMed: 15173585]
25. Conti M, Jin SL. The molecular biology of cyclic nucleotide phosphodiesterases. Prog Nucleic Acid Res Mol Biol. 1999; 63:1–38. [PubMed: 10506827]
26. Wang B, Fallon JF, Beachy PA. Hedgehog-regulated processing of Gli3 produces an anterior/posterior repressor gradient in the developing vertebrate limb. Cell. 2000; 100:423–434. [PubMed: 10693759]
27. Ruiz i Altaba A, Mas C, Stecca B. The Gli code: an information nexus regulating cell fate, stemness and cancer. Trends Cell Biol. 2007; 17:438–447. doi:10.1016/j.tcb.2007.06.007. [PubMed: 17845852]
28. Regard JB, et al. Activation of Hedgehog signaling by loss of GNAS causes heterotopic ossification. Nature medicine. 2013; 19:1505–1512. doi:10.1038/nm.3314.
29. Mukhopadhyay S, et al. The ciliary G-protein-coupled receptor Gpr161 negatively regulates the Sonic hedgehog pathway via cAMP signaling. Cell. 2013; 152:210–223. doi:10.1016/j.cell.2012.12.026. [PubMed: 23332756]
30. Yang L, et al. Blocking CXCR4-mediated cyclic AMP suppression inhibits brain tumor growth in vivo. Cancer research. 2007; 67:651–658. doi:10.1158/0008-5472.CAN-06-2762. [PubMed: 17234775]
31. Rohatgi R, Milenkovic L, Scott MP. Patched1 regulates hedgehog signaling at the primary cilium. Science. 2007; 317:372–376. doi:10.1126/science.1139740. [PubMed: 17641202]
32. Goetz SC, Ocbina PJ, Anderson KV. The primary cilium as a Hedgehog signal transduction machine. Methods in cell biology. 2009; 94:199–222. doi:10.1016/S0091-679X(08)94010-3. [PubMed: 20362092]
33. Chen JK, Taipale J, Young KE, Maiti T, Beachy PA. Small molecule modulation of Smoothened activity. Proceedings of the National Academy of Sciences of the United States of America. 2002; 99:14071–14076. doi:10.1073/pnas.182542899. [PubMed: 12391318]

34. Dijkgraaf GJ, et al. Small molecule inhibition of GDC-0449 refractory smoothened mutants and downstream mechanisms of drug resistance. Cancer research. 2011; 71:435–44. [PubMed: 21123452]
35. Schuller U, et al. Acquisition of granule neuron precursor identity is a critical determinant of progenitor cell competence to form Shh-induced medulloblastoma. Cancer cell. 2008; 14:123–134. [PubMed: 18691547]
36. Xin M, et al. Myelinogenesis and axonal recognition by oligodendrocytes in brain are uncoupled in Olig1-null mice. The Journal of neuroscience : the official journal of the Society for Neuroscience. 2005; 25:1354–1365. doi:10.1523/JNEUROSCI.3034-04.2005. [PubMed: 15703389]
37. Lu QR, et al. Sonic hedgehog--regulated oligodendrocyte lineage genes encoding bHLH proteins in the mammalian central nervous system. Neuron. 2000; 25:317–329. [PubMed: 10719888]
38. Machold R, Klein C, Fishell G. Genes expressed in Atoh1 neuronal lineages arising from the r1/isthmus rhombic lip. Gene expression patterns : GEP. 2011; 11:349–359. doi:10.1016/j.gep.2011.03.007. [PubMed: 21440680]
39. Gibson P, et al. Subtypes of medulloblastoma have distinct developmental origins. Nature. 2010; 468:1095–1099. [PubMed: 21150899]
40. Gilbertson RJ, Ellison DW. The origins of medulloblastoma subtypes. Annu Rev Pathol. 2008; 3:341–365. doi:10.1146/annurev.pathmechdis.3.121806.151518. [PubMed: 18039127]
41. Pounds S, et al. A procedure to statistically evaluate agreement of differential expression for cross-species genomics. Bioinformatics. 2011; 27:2098–2103. [PubMed: 21697127]
42. Tibshirani R, Hastie T, Narasimhan B, Chu G. Diagnosis of multiple cancer types by shrunken centroids of gene expression. Proceedings of the National Academy of Sciences of the United States of America. 2002; 99:6567–6572. doi:10.1073/pnas.082099299. [PubMed: 12011421]
43. Sengupta R, et al. CXCR4 activation defines a new subgroup of Sonic hedgehog-driven medulloblastoma. Cancer research. 2012; 72:122–132. doi:10.1158/0008-5472.CAN-11-1701. [PubMed: 22052462]
44. Northcott PA, et al. Subgroup-specific structural variation across 1,000 medulloblastoma genomes. Nature. 2012; 488:49–56. doi:10.1038/nature11327. [PubMed: 22832581]
45. Mishra PK, et al. Misregulation of Scm3p/HJURP causes chromosome instability in Saccharomyces cerevisiae and human cells. PLoS Genet. 2011; 7:e1002303. doi:10.1371/journal.pgen.1002303. [PubMed: 21980305]
46. Dunleavy EM, et al. HJURP is a cell-cycle-dependent maintenance and deposition factor of CENP-A at centromeres. Cell. 2009; 137:485–497. doi:10.1016/j.cell.2009.02.040. [PubMed: 19410545]
47. Parsons DW, et al. The genetic landscape of the childhood cancer medulloblastoma. Science. 2011; 331:435–439. doi:10.1126/science.1198056. [PubMed: 21163964]
48. Silbereis JC, et al. Olig1 function is required to repress dlx1/2 and interneuron production in Mammalian brain. Neuron. 2014; 81:574–587. doi:10.1016/j.neuron.2013.11.024. [PubMed: 24507192]
49. O'Hayre M, et al. The emerging mutational landscape of G proteins and G-protein-coupled receptors in cancer. Nature reviews. Cancer. 2013; 13:412–424. doi:10.1038/nrc3521. [PubMed: 23640210]
50. Romer JT, et al. Suppression of the Shh pathway using a small molecule inhibitor eliminates medulloblastoma in Ptc1(+/−)p53(−/−) mice. Cancer cell. 2004; 6:229–240. [PubMed: 15380514]
51. Yauch RL, et al. Smoothened mutation confers resistance to a Hedgehog pathway inhibitor in medulloblastoma. Science. 2009; 326:572–574. doi:10.1126/science.1179386. [PubMed: 19726788]
52. Sengupta R, Sun T, Warrington NM, Rubin JB. Treating brain tumors with PDE4 inhibitors. Trends Pharmacol Sci. 2011; 32:337–344. doi:10.1016/j.tips.2011.02.015. [PubMed: 21450351]
53. Chahar MK, Sharma N, Dobhal MP, Joshi YC. Flavonoids: A versatile source of anticancer drugs. Pharmacognosy reviews. 2011; 5:1–12. doi:10.4103/0973-7847.79093. [PubMed: 22096313]
54. Nikaido T, et al. Inhibition of adenosine 3′,5′-cyclic monophosphate phosphodiesterase by flavonoids. III. Chemical & pharmaceutical bulletin. 1989; 37:1392–1395. [PubMed: 2560949]
55. Ng JM, Curran T. The Hedgehog's tale: developing strategies for targeting cancer. Nature reviews. Cancer. 2011; 11:493–501. doi:10.1038/nrc3079.

56. Chen M, et al. Increased glucose tolerance and reduced adiposity in the absence of fasting hypoglycemia in mice with liver-specific Gs alpha deficiency. The Journal of clinical investigation. 2005; 115:3217–3227. doi:10.1172/JCI24196. [PubMed: 16239968]
57. Northcott PA, et al. Medulloblastoma comprises four distinct molecular variants. J Clin Oncol. 2011; 29:1408–1414. doi:10.1200/JCO.2009.27.4324. [PubMed: 20823417]
58. Northcott PA, et al. Rapid, reliable, and reproducible molecular sub-grouping of clinical medulloblastoma samples. Acta neuropathologica. 2012; 123:615–626. doi:10.1007/s00401-011-0899-7. [PubMed: 22057785]
59. Carvalho BS, Irizarry RA. A framework for oligonucleotide microarray preprocessing. Bioinformatics. 2010; 26:2363–2367. doi:10.1093/bioinformatics/btq431. [PubMed: 20688976]
60. Vilella AJ, et al. EnsemblCompara GeneTrees: Complete, duplication-aware phylogenetic trees in vertebrates. Genome Res. 2009; 19:327–335. doi:10.1101/gr.073585.107. [PubMed: 19029536]

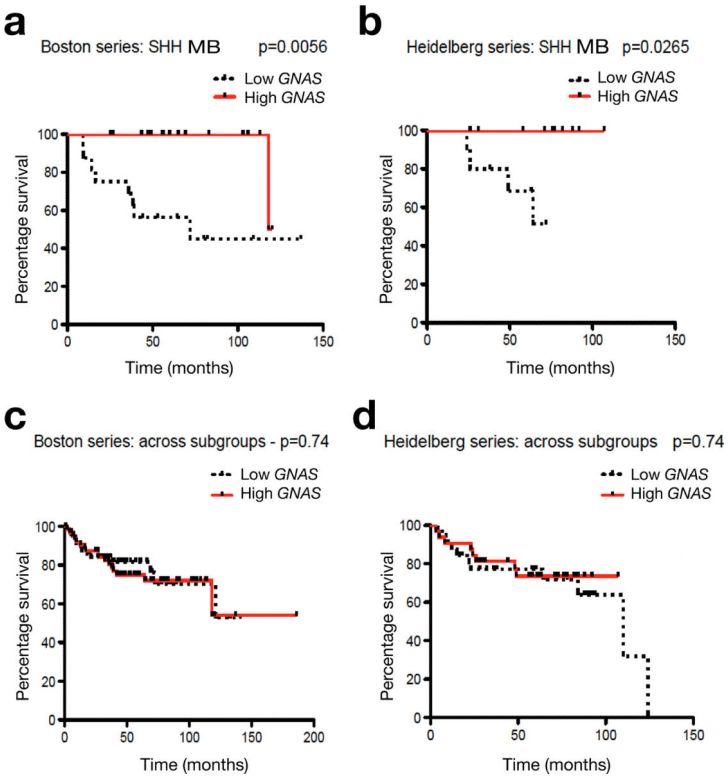

Figure 1. *GNAS* defines a subset of aggressive SHH-group tumors

(**a-d**) MB patients with available survival information and gene expression profiling studies from both Boston and Heidelberg series of MBs [10,11] were divided into two groups using the median *GNAS* expression value as the cutoff point. The relationship between *GNAS* mRNA expression and survival time was analyzed according to the Kaplan-Meier method, using log rank statistics. *GNAS* levels and patient numbers: **a**, low (*n* =16), high (*n* =17); **b**, low (*n* = 10), high (*n* = 10); **c**, low (*n* = 32), high (*n* = 32); **d**, low (*n* = 64), high (*n* = 65).

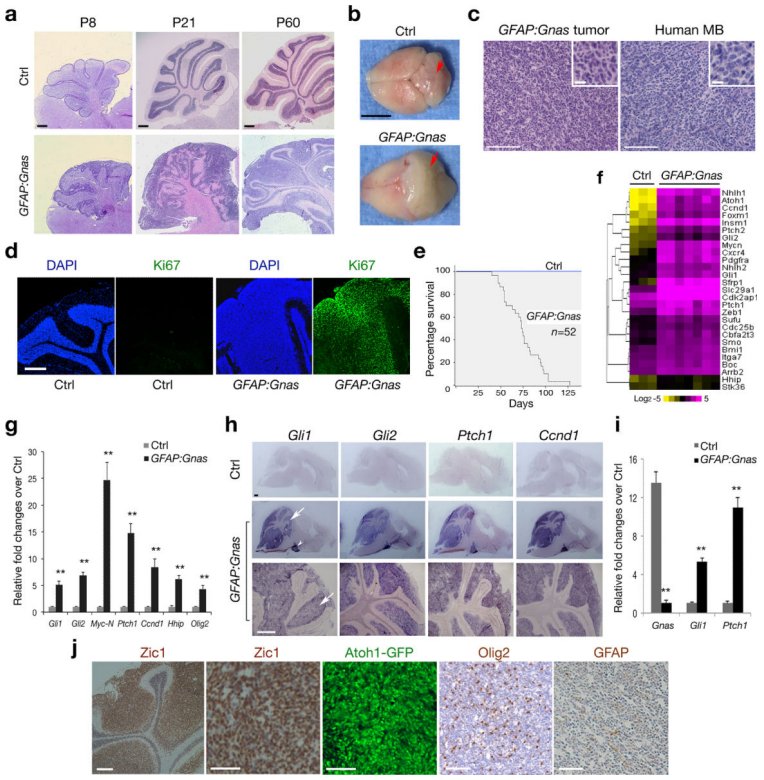

Figure 2. Loss of *Gnas* in neural stem/progenitor cells induces MB formation

(**a**) Sagittal brain sections from *hGFAPCre:Gnas*$^{lox/lox}$ (*GFAP:Gnas*) and *hGFAPCre:Gnas*$^{lox/+}$ (Ctrl) mice at indicated stages were stained with hematoxylin and eosin (H/E).

(**b**) Brain appearance of control and *Gnas* mutants at P67. The arrows indicate the cerebellum.

(**c**) Tumors from *Gnas* mutants (left) displays similar histology to human MB (right; SHH group). Insets are shown at high magnification.

(**d**) The cerebella of control and *Gnas* mutants at P60 were stained with anti-Ki67 and DAPI.

(**e**) Kaplan-Meier survival curves for control and *GFAP:Gnas* mice (n = 52).

(**f**) Heatmap shows expression of Shh pathway components in control cerebella and *GFAP:Gnas* tumor tissues. The color bar shows expression intensity.

(**g**) qRT-PCR quantification of *Gnas* and Shh pathway genes in control and *GFAP:Gnas* cerebella at P30. Data represent the mean ± SEM (n = six animals). ** $P < 0.01$; Student's t test.

(**h**) mRNA expression of Shh target genes as indicated in control and *GFAP:Gnas* brain sections at P60. Arrow and arrowhead indicate the cerebellum and pontine grey nucleus, respectively.

(**i**) qRT-PCR analysis of *Gnas*, *Gli1* and *Ptch1* in GNPs from control and *GFAP:Gnas* mice at P7. Data represent the mean ± SEM (n = five animals). ** $P < 0.01$; Student's t test.

(**j**) The cerebellar EGL region of *GFAP:Gnas* mice carrying the Atoh1-GFP reporter at P50 was immunostained with anti-Zic1, Olig2 and GFAP as indicated.

Scale bars in **a,** 300 μm; **b,** 5 mm; **c, d, h,** 200 μm; inset in **c**, 10 μm; **j,** 100 μm.

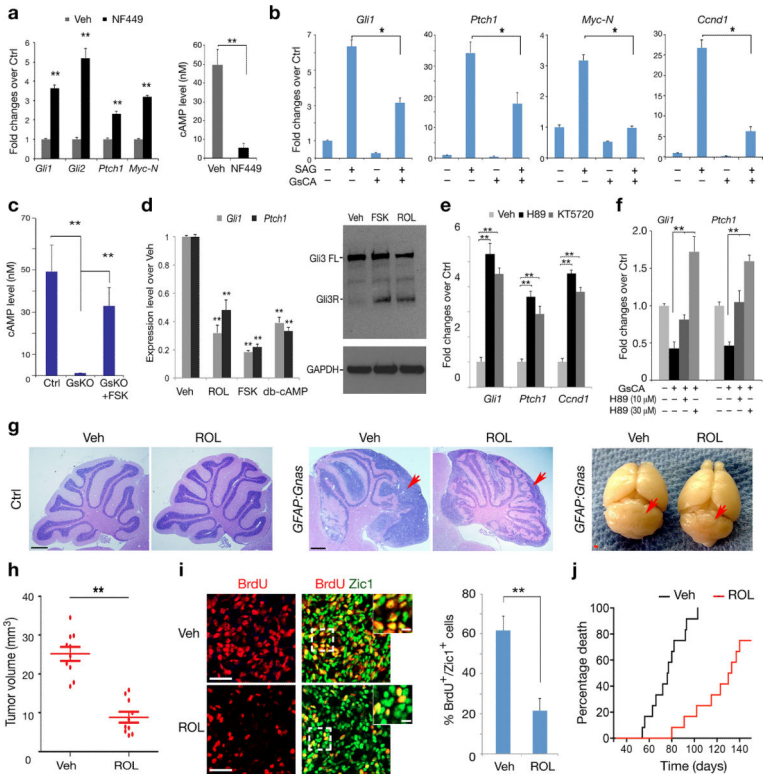

Figure 3. Gsα and its effector cAMP inhibit Shh signaling and tumor growth in *Gnas* mutants

(**a**) Bar graph (left) depicts expression changes in GNPs treated NF449 over control. Right: cAMP levels measured by ELISA.

(**b**) GNPs were treated with vehicle and SAG (200 nM) and/or transfected with pcDNA3 control and GsαQ227L (pGsCA) for 48 h. Bar graphs depict *Gli1* and *Ptch1* expression changes in treated cells over control.

(**c**) Average cAMP levels of control and mutant GNPs treated with vehicle and forskolin.

(**d**) GNPs were treated with vehicle or Rolipram (50 μM), forskolin (10 μM) and db-cAMP (100 μM) for 3 h. *Gli1* and *Ptch1* or Gli3FL and Gli3R were analyzed by qRT-PCR (left) and western blotting (right) as indicated. GAPDH: loading control.

(**e**) Quantification of *Gli1*, *Ptch1* and *Ccnd1* in GNPs treated with H89 or KT5720 over control.

(**f**) Bar graphs depict the relative fold change of *Gli1* and *Ptch1* expression in GNPs transfected with pGsCA with or without H89 treatment over control.

(**g**) Control and *Gnas* mice (*n* = eight for each group) were randomized to receive Rolipram or vehicle from P35 to P65. Representative images of H/E staining of cerebellar sections and brain morphology were shown. Arrows: the cerebellum.

(**h**) Scatter dot-plot depicts average tumor volumes estimated for vehicle- and Rolipram-treated *Gnas* mutants. Lines: mean values ± SEM.

(**i**) Images show immunostaining of Zic1 and BrdU in vehicle and Rolipram-treated *GFAP:Gnas* tumors at P65. Insets: high magnification in boxed areas. Bar graph (right) depicts the percentage of $BrdU^+/Zic1^+$ cells (*n* = eight animals each group).

(**j**) Kaplan-Meier survival curves for *GFAP:Gnas* mice (n = 12 per group) were randomized to receive Rolipram or vehicle at P30 for six weeks. P value for the log-rank test =0.0071. Scale bars in **g**, 300 μm; **i**, 20 μm (insets 4 μm). Data shown in **a**-**f** are the mean ± SEM representing at least three independent experiments. *$P < 0.05$, ** $P < 0.01$; Student's t-test.

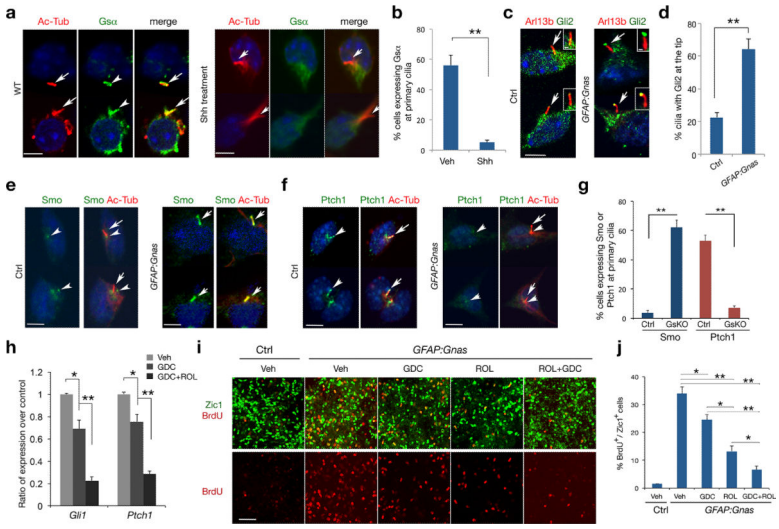

Figure 4. Gsα regulates ciliary trafficking of hedgehog signaling components in GNPs

(**a-b**) GNPs without or with Shh treatment (3 μg ml^{-1}) for 16 hr were immunostained with anti-Gsα and acetylated α-tubulin (Ac-Tub) (arrows). **b**: quantitation of Gsα fluorescence at the primary cilium (≥ 300 cell counts each group per experiment).

(**c-g**) GNPs from control or *GFAP:Gnas* mice were immunostained with anti-Gli2, Smo, Ptch1 and Ac-Tub. Insets in **c** show cilia at a high magnification. Bar graphs in **d**, **g** depict the percentage of Gli2 accumulation at cilium tips, and Smo or Ptch1 fluorescence at the primary cilium, respectively (≥ 300 cell counts per genotype from each experiment). Arrows and arrowheads indicate primary cilia and their base, respectively.

(**h**) GNPs from *Gnas* mutants were treated with GDC-0449 (1 μm) or both GDC-0449 and Rolipram (50 μm). Bar graphs depict relative *Gli1* and *Ptch1* expression by qRT-PCR in drug-treated vs. vehicle-treated cells.

(**i**) Zic1 and BrdU immunostaining in GNPs from *Gnas* mutants treated GDC-0449, Rolipram or both and labeled with BrdU for 48 hr.

(**j**) Bar graph depicts the average percentage of $BrdU^+$ cells among $Zic1^+$ GNPs.

Experiments were performed three times with at least $n = 3$ for each treatment. One-way ANOVA with post hoc Newman–Keuls multiple comparison test. $^{**}P < 0.01$.

Scale bars in **a-f**, 3 μm; **c** insets, 0.5 μm; **i**, 30 μm. Representative images and quantifications from at least three independent experiments are shown. Data represent the mean ± SEM. $^{*}P < 0.05$, $^{**}P < 0.01$, Student's *t*-test or one-way ANOVA.

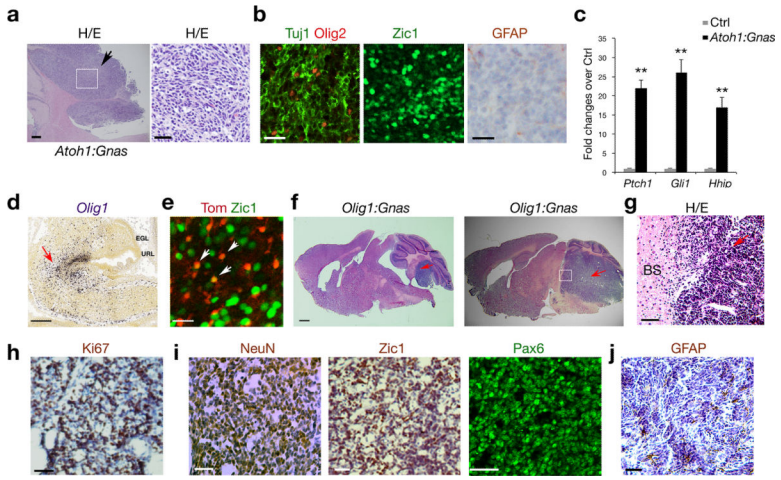

Figure 5. Loss of *Gnas* in *Atoh1*$^{+}$ or *Olig1*$^{+}$ progenitors leads to an anatomically distinct Shh-associated MB

(**a**) A sagittal hindbrain section from a *Atoh1:Gnas* mouse at P50 was stained with H/E. The boxed area is shown at a high magnification in the right panel.

(**b**) Tumor tissues were immunostained with anti-Tuj1, Olig2, Zic1 and GFAP as indicated.

(**c**) Bar graphs depict expression of *Ptch1*, *Gli1* and *Hhip* in *Atoh1:Gnas* cerebella over control at P40. Data represent the mean ± SEM from five animals each group. ** $P < 0.01$; Student's *t* test.

(**d**) *Olig1* expression (arrow) was detected in the progenitors of the dorsal brainstem at sagittal levels at E15.5 by *in situ* hybridization.

(**e**) The dorsal brainstem region from *Olig1-Cre*:Rosa-tdTomato mice at P7 was immunostained with Zic1. Arrows indicates a population of tdTomato^{+} cells Zic1.

(**f-g**) H/E staining of the sagittal sections of *Olig1:Gnas* brains at 3 or 5 month ages. Arrows indicate the tumor tissue. Boxed region in **f** is shown at high magnification in **g**. BS: brainstem.

(**h-j**) Sections of *Olig1:Gnas* tumor tissues were immunostained with anti-Ki67, NeuN, Zic1, Pax6 and GFAP as indicated.

Scale bars in **a**, 50 μm. **b**, 20 μm, **d**, **f**, 200 μm; **e**, 20 μm; **g-j**, 50 μm.

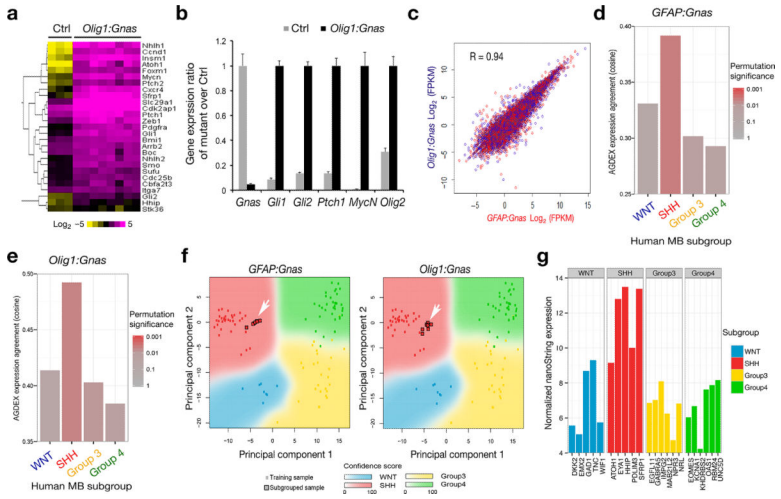

Figure 6. Tumors in *Gnas* mutants exhibit a gene expression signature resembling SHH-MB

(**a**) Heatmap analysis of gene profiling of control cerebella (n = 3) and tumor tissues (n = 8) from *Olig1:Gnas* mutants by RNA-sequencing shows upregulation of Shh pathway components in tumors. The color bar shows expression intensity.

(**b**) Relative expression of Shh pathway components between control and *Olig1:Gnas* tumors from four month old animals (n = eight per group) was assayed by qRT-PCR. ** $p <$ 0.01; Student's t test.

(**c**) Regression analysis of gene expression profiles indicates a direct correlation of gene transcription profiles between *GFAP:Gnas* and *Olig1:Gnas* tumors (n = eight per group).

(**d-e**) Cross-species comparison of global differential expression from Affymetrix microarray analysis of mouse tumors (n = eight per group) with bona fide human MB subgroups by AGDEX3 R algorithm. Bar graphs represent the cosine similarity measure and reflect the similarity of global expression profile between each mouse tumor subtype and each human MB subgroup.

(**f**) Principal component analysis (PCA) of expression profiles between human and above mouse tumor samples. Arrows indicate that gene expression profiles of mouse tumors match to Shh-subgroup.

(**g**) Subgrouping analysis by nanoString technology indicates the MB from the patient with a *GNAS* homozygous nonsense mutation resembles a SHH-group tumor with high confidence (PAM prediction score = 0.999996).